Transforming Liquid Nicotine into a Stable Solid Through Crystallization with Orotic Acid

Journal:	*CrystEngComm*
Manuscript ID	CE-ART-06-2022-000764.R1
Article Type:	Paper
Date Submitted by the Author:	22-Jul-2022
Complete List of Authors:	Angevine, Devin; University at Buffalo College of Arts and Sciences, Chemistry Department Camacho, Kristine; University at Buffalo College of Arts and Sciences, Chemistry Department Rzayev, Javid ; University at Buffalo College of Arts and Sciences, Department of Chemistry Benedict, Jason; University at Buffalo College of Arts and Sciences, Chemistry Department

ARTICLE

Transforming Liquid Nicotine into a Stable Solid Through Crystallization with Orotic Acid

Received 00th January 20xx,
Accepted 00th January 20xx

DOI: 10.1039/x0xx00000x

Devin J. Angevine,[a] Kristine Joy Camacho,[b] Javid Rzayev [c] and Jason B. Benedict *[d]

Abstract: Many molecular drugs exist as liquid materials, however this state is not necessarily the most viable or stable means to store pharmaceuticals. Crystal engineering can be utilized to isolate these liquid materials in the solid state. Herein, we describe the liquid-state to solid-state transformation of one of the most widely consumed liquid alkaloid drugs; nicotine. Nicotine is known to be highly unstable with a multitude of degradation pathways. To isolate nicotine in the solid-state, crystallization was utilized with the generally recognized as safe (GRAS) salt former orotic acid. The melting point of the isolated crystalline salt was determined along with the photo-stabilizing effects the solid state offers for liquid pharmaceuticals such as nicotine.

Introduction

In drug design, the solid-state is often targeted during development for active pharmaceutical ingredients (APIs) due in part to its relative stability over other forms, such as the liquid-state.[1] Liquid and solution-based APIs tend to be less stable at ambient conditions, with a range of degradation modes that prove troublesome for handling and storage. One such mode of degradation arises from ambient oxygen exposure that can oxidize molecules, such as propofol.[2] As such, propofol formulation has been investigated to isolate this liquid anaesthetic into the solid-state, as it is on the WHO Model List of Essential Medicines.[3, 4]

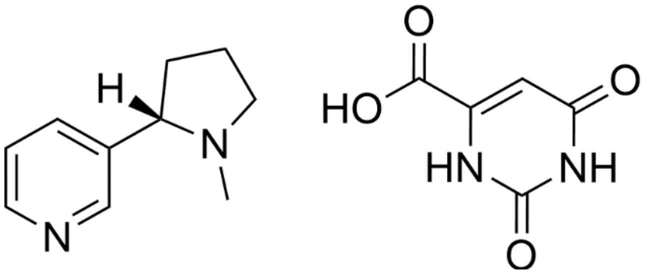

Figure 1: Chemical structures of the API nicotine (left) and the salt former orotic acid (right).

Many pharmaceuticals are known to exhibit sensitivity or degradation upon light exposure, including numerous solution-based drugs such as doxycycline hyclate and ephedrine sulfate.[5] Both of these drugs have special storage conditions, including amber vials and instructions to store away from light to prevent photodegradation.[6]

Characterized as an oily pale-yellow liquid, with a density akin to that of water, nicotine is a small organic compound that has notoriety across the globe due to being the API in tobacco products. Pure liquid nicotine is, however, plagued by degradation issues. Similar to the previously described APIs, nicotine is known to decompose upon exposure to light or air into oxynicotine, nicotinic acid and methylene.[7, 8] Degradation products such as nicotinic acid pose relatively little harm, while others such as the reactive diradical methylene possess the ability and reactivity to cause further unwanted downstream interactions.[9]

In addition to the issues nicotine faces as a pure liquid compound, salt formulations that are currently available have a range of issues also associated with them. Currently the most popular nicotine salt, nicotinium benzoate: a liquid formulation, is used with a cocktail of other chemicals such as carrier fluids and additives. These compounds have shown to form significant levels of benzene, a known carcinogen, when used in conjunction with widely

---

[a] *Department of Chemistry, University at Buffalo*
730 Natural Sciences Complex, Buffalo, 14260-3000, USA
[b] *Department of Chemistry, University at Buffalo*
838 Natural Sciences Complex, Buffalo, 14260-3000, USA
[c] *Department of Chemistry, University at Buffalo*
826 Natural Sciences Complex, Buffalo, 14260-3000, USA
[d] *Department of Chemistry, University at Buffalo*
771 Natural Sciences Complex, Buffalo, 14260-3000, USA
Electronic supplementary information (ESI) available. CCDC 2161823. For ESI and crystallographic data in CIF or another electronic format see DOI: 10.1039/x0xx00000x

available electronic delivery systems.[10] Crystallization offers the opportunity to isolate nicotine as a salt or co-crystal, thereby eliminating the requirement of carrier fluids or other additives.

As such, solid-state nicotine formulation has started to garner both academic and industrial interest.[11-16] Through the utilization of crystal engineering, it has been demonstrated that nicotine can be isolated in the solid-state crystalline form.[17] The crystalline solids isolated by Capucci *et al*. are not suitable for human consumption; however, as they contain coformers that are heavily halogenated or otherwise unsafe. Crystal engineering with coformers or salt formers that are suitable for human consumption presents an opportunity to isolate nicotine co-crystals and salts with improved degradation properties and potentially tune other properties of interest through the coformer or salt former selection.

To select a salt former suitable for this task, food safe, flavor additive, and generally recognized as safe (GRAS) coformers and salt formers were inspected.[18-21] GRAS substances are compounds that the US FDA has tested and affirmed as being safe for human consumption.[22, 23] Previously, malic acids were investigated for their ability to isolate nicotine in the solid-state through crystal engineering.[24] In this work, orotic acid, formerly known as vitamin B13, was selected as the salt former of interest.[24] Orotic acid is a naturally occurring compound that is often used as a supplement and may possess health benefits, such as improved heart health.[25] As salt formation is targeted in this work, the large ΔpK_a of 5.19 was successfully predicted to promote the necessary proton transfer between the orotic acid (pK_a = 2.83) and basic nicotine (pK_a = 8.02), according to the pK_a rule often observed for acid-base crystalline complexes.[26]

Results and Discussion

Nicotinium Orotate Structural Characterization

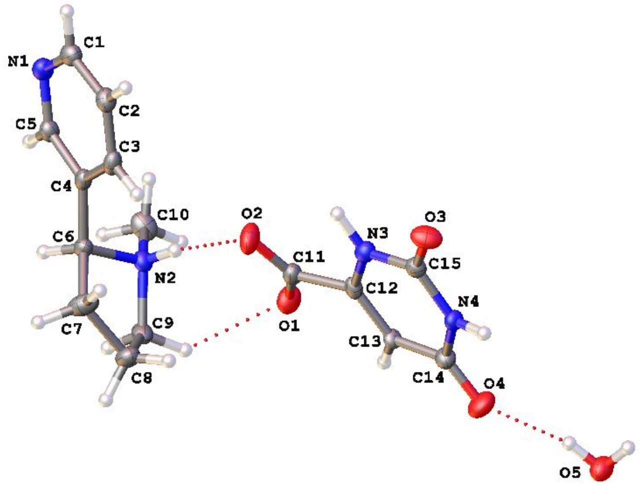

Figure 2: Asymmetric unit of (S)-nicotinium orotate hemihydrate. Atom colors: oxygen (red), nitrogen (blue), carbon (grey), hydrogen (white). Hydrogen bond interactions highlighted in red dashed lines.

When nicotine and orotic acid in a 1:1 stoichiometric ratio underwent slow evaporation from water, single crystals were formed containing a hydrated 1:1 ratio of nicotinium and orotate, with the salt crystalizing in the orthorhombic spacegroup $P222_1$. (Figure 2). Within the asymmetric unit of the salt, the oxygen atom of the water molecule was found to reside on a special position, a C_2 rotation axis parallel to [010]. Thus, the water molecule oxygen only contributes half site occupancy to the asymmetric unit, making this salt a hemihydrate.

Formation of the salt was confirmed through refinement and analysis of the crystal structure. After refinement of heavy atoms, the Fourier differences map revealed a q-peak approximately 0.9 Å from N2 in the direction of O2 consistent with protonation of N2. The C11-O1 and C11-O2 bond lengths were determined to be nearly identical at 1.24 Å and 1.26 Å, respectively, indicating the acid group is deprotonated to give the corresponding carboxylate.

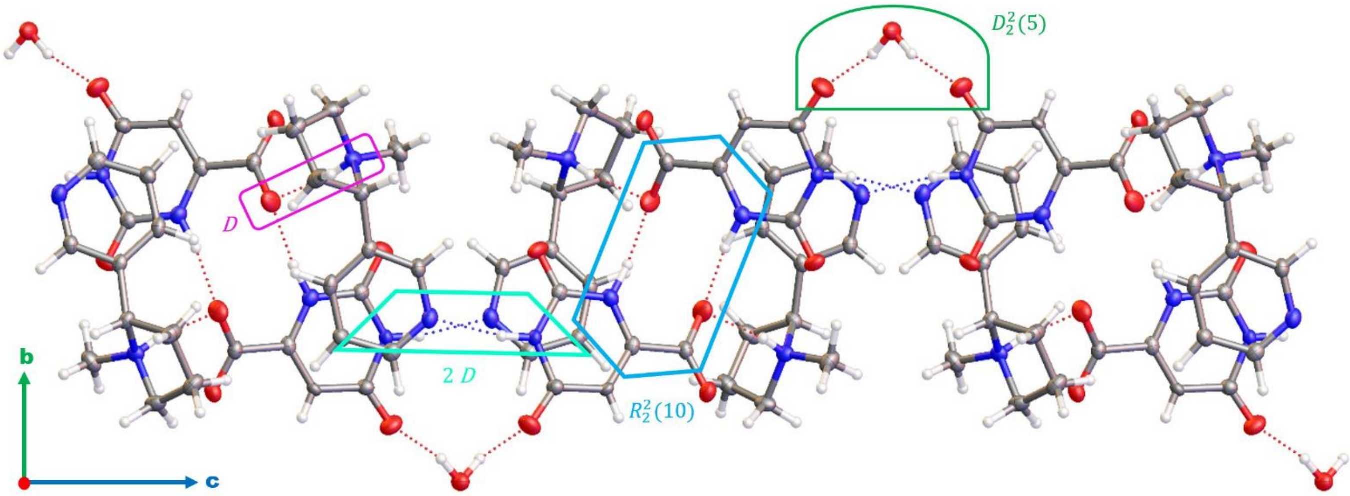

Figure 3: A single sheet of (S)-nicotinium orotate hemihydrate with bonding interaction motifs depicted. Hydrogen bonding interactions are highlighted via dashed red and blue lines. Atom colors: oxygen (red), nitrogen (blue), carbon (grey), hydrogen (white).

Table 1: Hydrogen bond distances and geometries for (S)-nicotinium orotate hemihydrate with associated ESDs.

Interacting Atoms (D—H···A)	D—H Distance (Å)	H···A Distance (Å)	D···A Distance (Å)	D—H···A Angle (°)
C13—H13···O1$^{\text{ii}}$	0.95	2.17	3.070 (4)	158
C5—H5···O3$^{\text{iii}}$	0.95	2.65	3.338 (4)	130
C9—H9A···O1$^{\text{iv}}$	0.99	2.40	3.085 (4)	126
C10—H10C···O3	0.98	2.33	3.185 (5)	146
C8—H8B···O1$^{\text{v}}$	0.99	2.61	3.297 (5)	127
C7—H7B···O3$^{\text{vi}}$	0.99	2.66	3.245 (5)	118
N4—H4···N1$^{\text{iii}}$	0.89 (4)	1.98 (4)	2.860 (4)	170 (3)
N2—H2···O1$^{\text{iv}}$	0.83 (4)	2.60 (4)	3.092 (4)	119 (3)
N2—H2···O2$^{\text{iv}}$	0.83 (4)	1.93 (4)	2.758 (4)	172 (4)
N3—H3A···O2$^{\text{iv}}$	1.02 (4)	1.96 (4)	2.950 (4)	166 (4)
O5—H5A···O4$^{\text{vii}}$	0.86 (4)	1.97 (4)	2.798 (3)	163 (4)
Symmetry codes: (ii) x, −y+2, −z+1; (iii) −x+1, y, −z+1/2; (iv) x, −y+1, −z+1; (v) x−1, −y+1, −z+1; (vi) x−1, y, z; (vii) x−1, y−1, z.				

Nicotinium orotate hemihydrate contains a number of unique hydrogen bonding interactions including orotate-orotate, orotate-nicotinum, and orotate-water interactions. The water molecule, which resides on a C_2-axis, forms $D_2^2(5)$ interactions, with two symmetry equivalent hydrogen bonds to orotate with a distance between the ketone oxygen of the orotate and the oxygen of the water molecule of 2.798(3) Å. Intermolecular hydrogen bonding was observed between the carboxylate of the orotate and pyrrolidyl group on the nicotinium. This *D* motif hydrogen bonding interaction exhibited a distance of 2.758(4) Å between heteroatoms (Figure 3).

Two symmetry related orotate anions form an $R_2^2(10)$ hydrogen bonding interaction. This ring is formed by a pair of 2.950(4) Å N-H---O type hydrogen bonding interactions (Figure

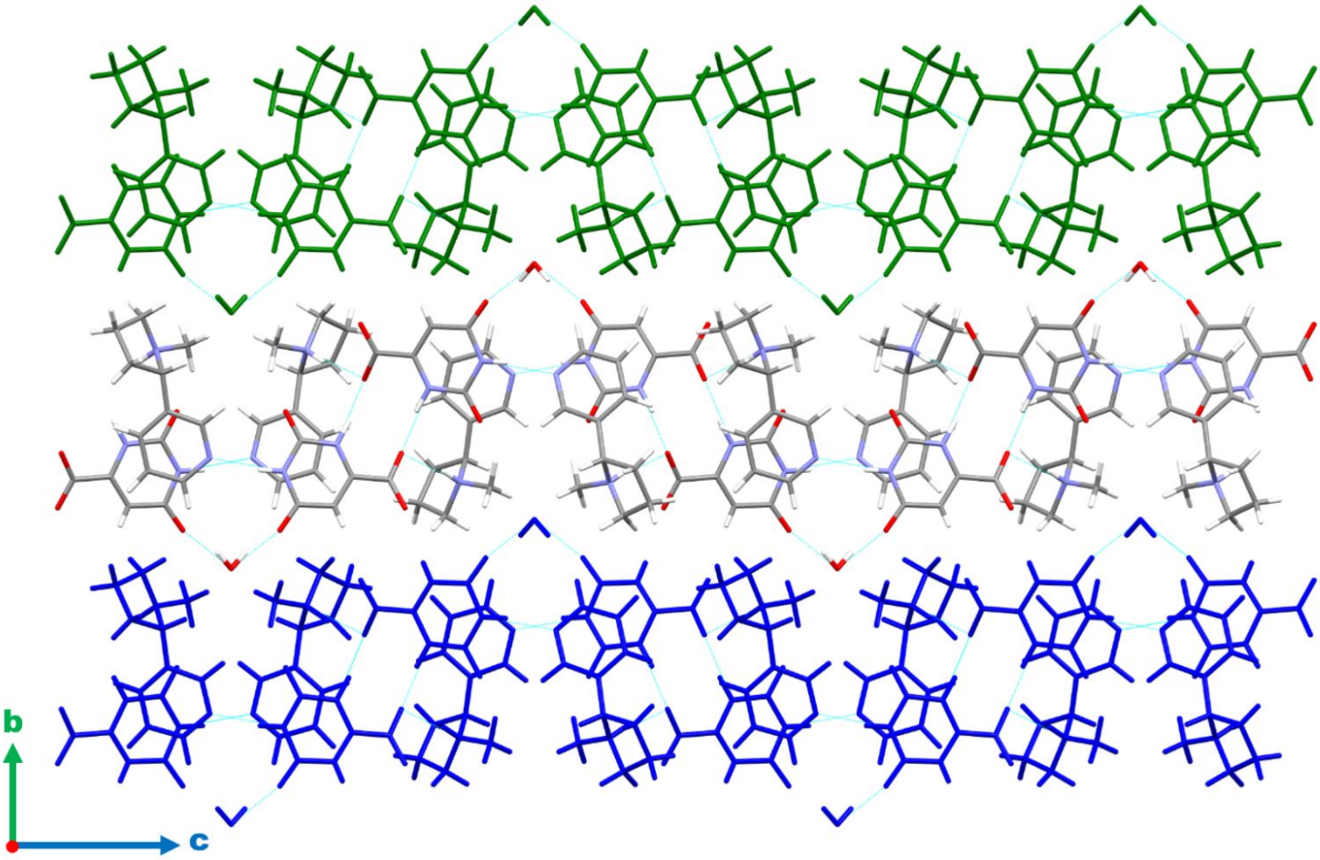

Figure 4: Diagram of edge-on view of hydrogen bonded *ac*-plane highlighting stacking of layers along [010]. Hydrogen bonding interactions highlighted via dashed blue lines. Atom colors in the middle sheet: oxygen (red), nitrogen (blue), carbon (grey), hydrogen (white). Atom colors in the bottom sheet are blue. Atom colors in the top sheet are green.

3). The secondary amine that is para to the carboxyl group of the orotate interacts with a neighboring orotate carboxyl oxygen. Details of the hydrogen bonding interactions are presented in Table 1. This complex array of interactions forms layers that run along [100] and then stack through Van der Waals interactions along [010] (Figure 4)

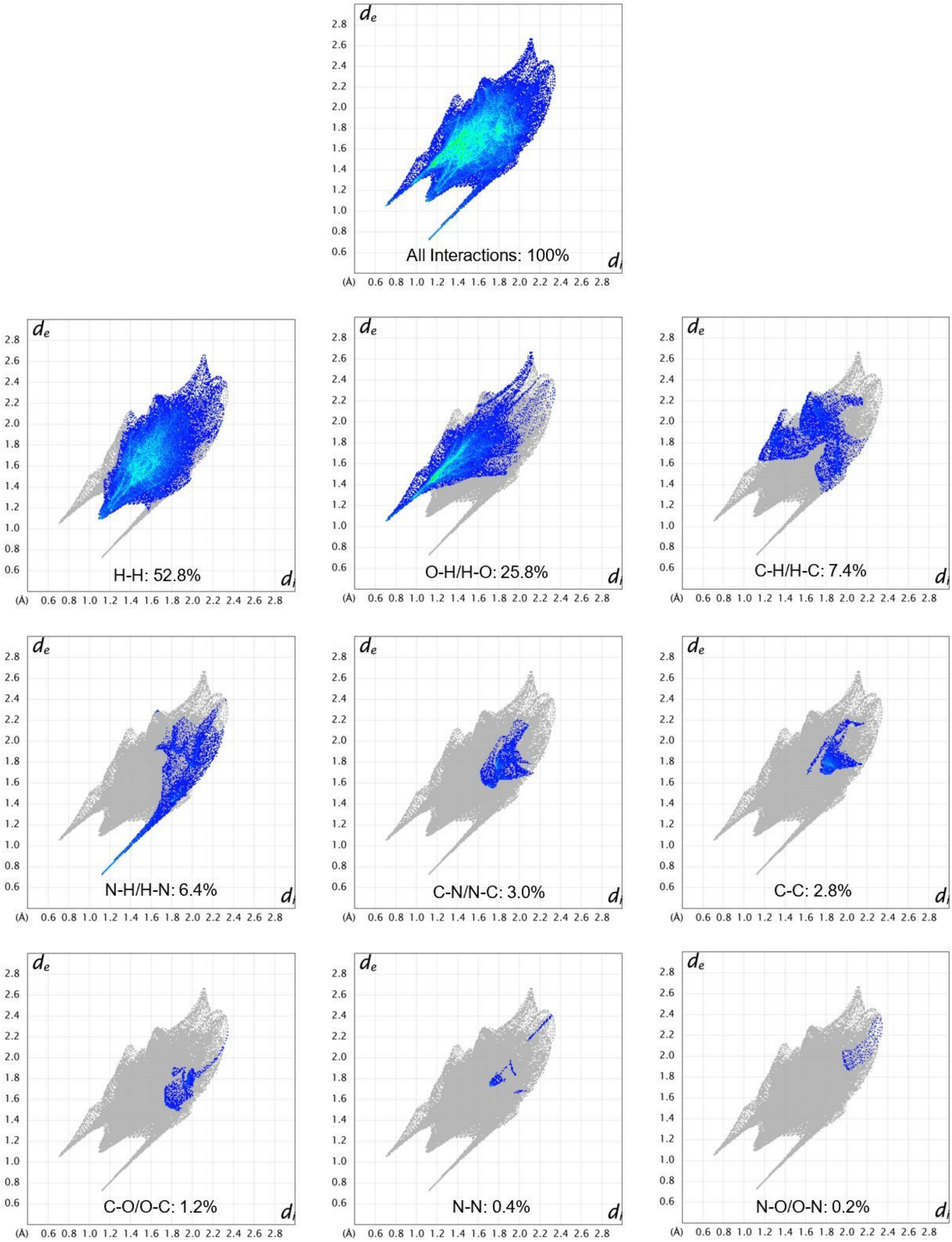

Figure 5: 2-D fingerprint plots of the (S)-nicotinium orotate hemihydrate salt. Interaction type and fraction relative to total is indicated in the lower portion of each image.

Hirshfeld Surface Analysis & Comparison

Hirshfeld surfaces remain an important tool for characterizing intermolecular interactions, including electrostatic potential, shape index and curvature, or d_{norm}, in crystalline systems.[27-29] The quantification of these properties provides insight into the nature and abundance of interactions within the lattice that is useful in understanding the interaction environment of an API and as such prove useful in designing future materials with the API.[30] The Hirshfeld surfaces are provided as video files in the ESI.

The interaction environment of (S)-nicotinium was analyzed for the orotate salt described herein, and several previously reported nicotinium malate salts to enable direct comparisons across these related systems. Nine types of interactions were observed in the novel salt described herein. Of these, 52.8% were H-H type interactions, 25.8% were O-H/H-O type interactions, 7.4% were C-H/H-C type interactions, 6.4% were N-H/H-N type interactions, 3.0% were C-N/N-C type interactions, 2.8% were C-C type interactions, 1.2% were C-O/O-C type interactions, 0.4% were N-N type interactions, and lastly 0.2% were N-O/O-N type interactions (Figure 5).

As observed in Figure 5, there are three distinct spikes observed in the short interaction region of the fingerprint plots. Numerous H-H interactions occur between the nicotinium and surrounding orotate, water and adjacent nicotinium molecules and are responsible for the center spike located at approximately 1.1 Å d_i × 1.1 Å d_e. A larger spike located at 0.7 Å d_i × 1.1 Å d_e corresponds to O-H/H-O interactions arising from short contacts between oxygen atoms on the orotate anion and pyrrolidinium and methyl group protons. In addition, a close interaction is observed between the nicotinium and a ketone from the adjacent salt former. The third observed large spike that peaks around 1.1 Å d_i × 0.7 Å d_e corresponds to the N-H/H-N interactions that are present. The shortest N-H/H-N interaction occurs at the pyridine ring of the nicotinium, wherein a hydrogen bonding interaction occurs between the nitrogen and amine from an adjacent orotate molecule. The C-H/H-C interactions are represented by a significant portion towards the center of the fingerprint. These interactions while present in abundance, do not show interactions as short as the other types discussed above as they are distributed around the edges of the nicotinium ring systems that are present.

In order to compare the interaction environment of the orotate salt to the malate salts, Hirshfeld surfaces and fingerprint plots were created using the CIF files available on the Cambridge Structural Database (REF codes: QAXQOZ, QAXQOZ01, QAXQOZ02, and QAXRAM). Surfaces based upon d_{norm}, the distance between the inner molecule of interest (d_i) and the outer exterior molecules (d_e), with respect to the Van der Waals radii, for the malate family of nicotine salts are presented in Figures S16-S19. Red and blue regions correspond to shorter and longer distances between the nuclei, respectively.

Figure 6 illustrates the percentage of each interactions type present in the malate family of salts as well as the orotate salt described herein. The four most abundant interaction types are conserved for these salts. Across all malate salts and nicotinium orotate salt, the most abundant interactions type was H-H interactions, followed by H-O/O-H type interactions, then C-

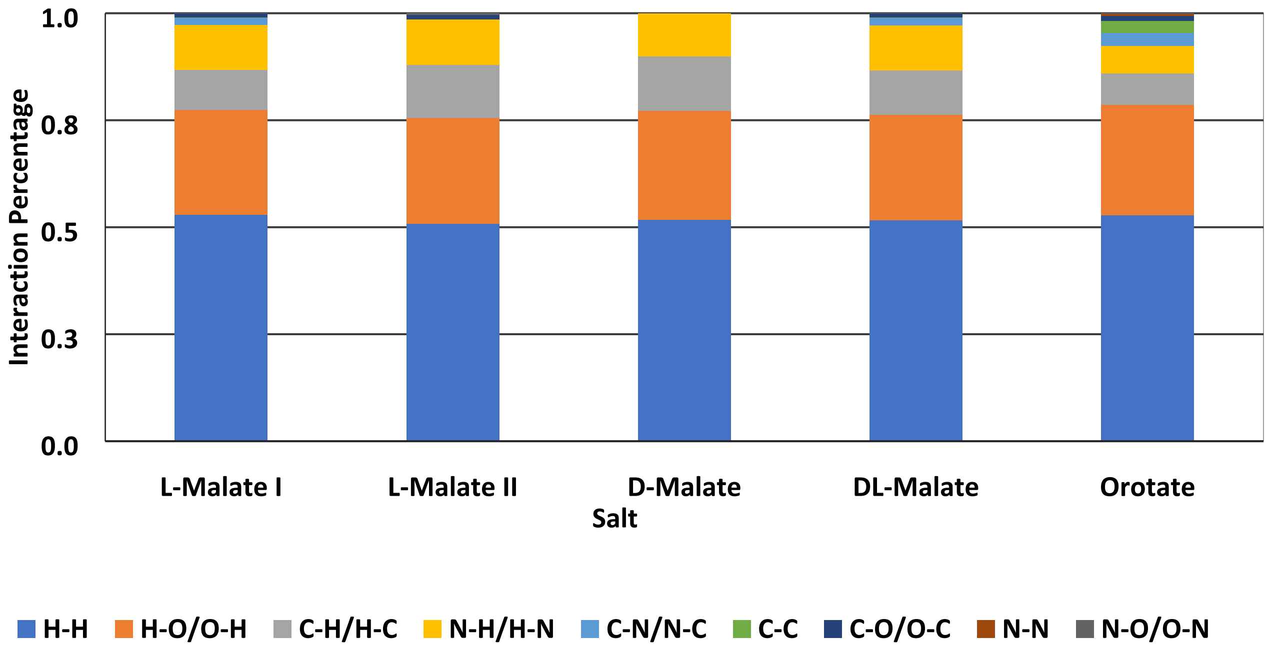

Figure 6: Interaction types and percentages for the nicotinium orotate salt described herein in comparison to the family of malate salts that has previously been synthesized. All percentages were acquired through Hirshfeld surface calculations using *Crystal Explorer 17.5*.

H/H-C type interactions and lastly N-H/H-N type interactions. The malate salts possessed a range of 50.8% - 52.9% for H-H interactions and the orotate salt also fell within that range with 52.8% of interactions present being H-H type. Likewise, the nicotinium in the orotate salt possessed a similar abundance of H-O/O-H type interactions (25.8%) when compared to the nicotinium in the malate salts (24.5% - 25.4%). The C-H/H-C type interactions present around the nicotinium in the orotate salt accounted for 7.4% of the total interactions, only slightly lower than the range of C-H/H-C interactions present around the nicotinium in the malate salts (9.4% - 12.7%). A similar result was observed when comparing the N-H/H-N type interactions as the orotate salt's nicotinium moiety possessed 6.4% of the total interactions which were present, while the nicotinium molecules in the malate salts had a slightly higher range of 10.1% - 10.7%. Additionally, the orotate salt described herein possesses several interactions not found in the malate salts, notably N-N and C-C, ostensibly due to the planar geometry of the heterocyclic salt former.

Thermal Characterization

As observed in the nicotinium malate salts, each salt possesses unique thermal properties, even among polymorphs and similar salts created using only different enantiomers.[24] Understanding the thermal properties of such crystalline systems can be useful in rationally designing and engineering similar materials in the future.[31] The melting point was determined by a digital melting point apparatus, as well as by differential scanning calorimetry (DSC). Upon heating to approximately 135 °C, nicotinium orotate hemihydrate melts into an amorphous material similar to other previously reported salts.[17, 24] The salt had an observable melting point range of 132 °C - 135 °C on the digital melting point apparatus, while an endothermic peak was observed at 135.5 °C via DSC. The enthalpy of fusion (ΔH°_{fusion}) was determined to be 26.24 kJ/mol (Table 2).

Table 2: Thermodynamic properties of nicotinium orotate hemihydrate.

Stuart SMP10 Melting Point (°C)	**DSC Endotherm Melting Point** (°C)	ΔH°_{fusion} (J/g)	ΔH°_{fusion} (kJ mol^{-1})	ΔS°_{fusion} (kJ mol^{-1} K^{-1})
132-135	135.5	80.16	26.24	6.421×10^{-2}

In the nicotinium malate salts, melting points determined via differential scanning calorimetry were observed as ranging from 93.4 °C - 122.2 °C, with enthalpies of fusion ranging from 11.22 kJ mol^{-1} to 18.62 kJ mol^{-1}.[24] Meanwhile, the nicotine co-crystals possessed melting points ranging between 54 °C to 92 °C, with ΔH°_{fusion} values ranging from 24.3 kJ/mol to 37.9 kJ/mol. Nicotinium orotate hemihydrate has a higher melting point than any of the four nicotinium malate salts as well as the nicotine containing co-crystals. The enthalpy of fusion of the nicotinum orotate salt is larger than that of any of the previously reported nicotine salts, yet remains lower than some nicotine-containing co-crystals. The higher melting point and enthalpy of fusion, relative to other nicotine salts, is likely due to the extensive hydrogen bonding network found in the nicotinium orotate salt.

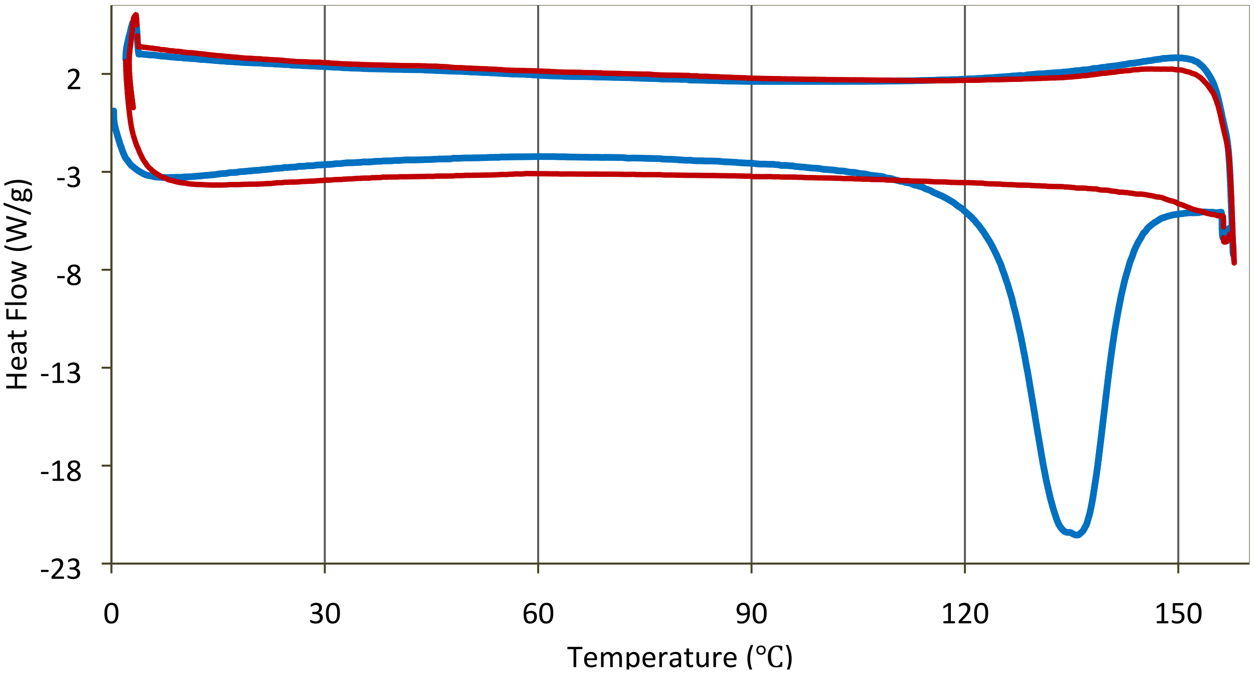

Figure 7: Differential scanning calorimetry data showing two scans of the orotate salt with exothermic processes having positive heat flow. The first scan is depicted with a solid blue line and the second scan is shown with a dashed red line. An endothermic transition associated with melting is observable in the first scan, while the second scan depicts no distinct or discernible thermal events.

As a measure of performance, the resulting salt melting points were compared to the orotic acid melting point (T_m), with the difference being reported as ΔT_m. This is done in a similar fashion to the previously reported halogenated nicotine cocrystals by Capucci *et al*. and similarly to the nicotinium malate salts. The salt reported herein exhibits an increased ΔT_m between the non-API salt former and the resulting crystalline material compared to previous reports. Orotic acid has a melting point that is not yet reported by NIST and as such a DSC scan was utilized to determine the endothermic transition corresponding to the melting point of orotic acid (Figure S15) . This value was determined to be 350.9 ℃ and was thusly utilized in the ΔT_m calculation. Subsequently, nicotinium orotate hemihydrate was found to possess a ΔT_m value of 215.4 °C; the highest reported value so far in literature. Such a large ΔT_m value is significantly different from other nicotine salts and co-crystals; for example, the nicotinium malate salts exhibited ΔT_m values ranging between 5.0 ℃ and 33.8 ℃, while the halogenated nicotine co-crystals were shown to possess a ΔT_m range of 55 ℃ to 78 ℃. However, like previous crystalline systems, orotic acid stabilized nicotine from its -79 ℃ melting point to a much greater melting point.

UV Photodegradation Testing

Pure liquid (S)-nicotine in its freebase form is known to degrade upon exposure to light, air, and moisture.[32] Upon ultraviolet (UV) light exposure nicotine undergoes decomposition into an oxidized form of nicotine known as nicotine N-oxide, nicotinic acid (vitamin B3), and methylamine.[33] The crystalline-state offers the potential to reduce the formation of such degradation products by restricting molecular motion of the API and reducing of the rate of molecular oxygen diffusion. Thus, the crystallization of nicotine provides an effective means of isolating and stabilizing nicotine compared to the pure liquid form. Such stability ought to improve the shelf life and storage conditions required for nicotine.

The photostability of the synthesized salt was assessed by placing a sample in a UV photoreactor for 24 hours. Following irradiation, a representative portion of the sample (10 mg) was collected for analysis via ^{1}H-NMR spectroscopy. The spectrum

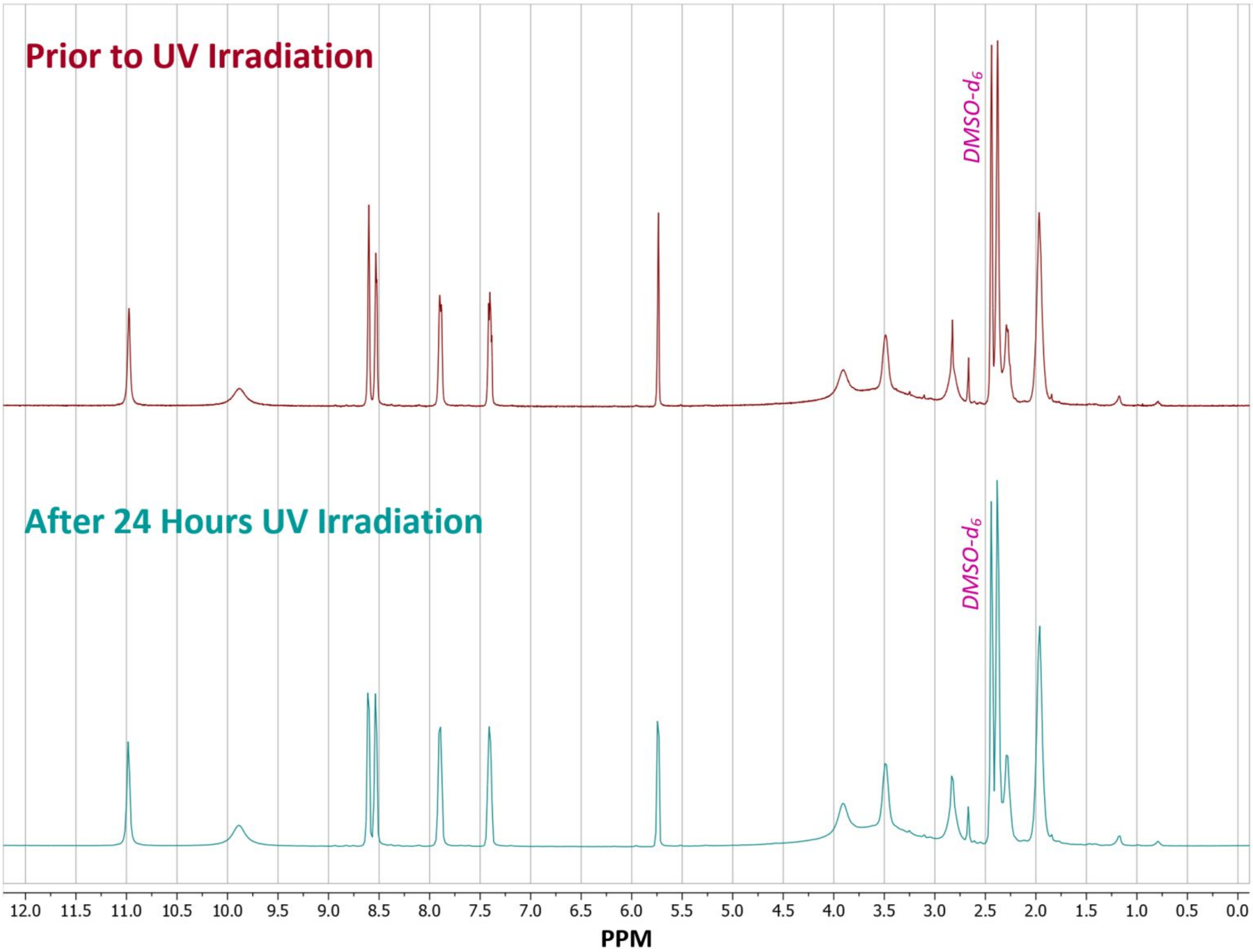

Figure 8: ^{1}H-NMR spectra of dimethyl sulfoxide-d_6 (DMSO-d_6) solutions of (S)-nicotinium orotate hemihydrate prepared from samples in which the crystalline phase received either no UV irradiation (upper) or 24 hours of UV irradiation (lower).

acquired after irradiation was compared to a spectrum from a sample collected prior to irradiation and analyzed to assess the extent of light-induced degradation. Pure nicotine as well as the orotic acid salt former were tested to establish controls for the salt former and the API.

The salt former, orotic acid, showed no detectable degradation after irradiation, whereas a sample of (S)-nicotine did exhibit many new peaks confirming that the neat API undergoes degradation when exposed to a UV light source. The pre- and post-irradiation spectra of nicotinium orotate hemihydrate were virtually identical indicating no detectable decomposition had occurred (Figure 8). The results are consistent with similar experiments involving nicotinium malate salts in which no detectable degradation was observed after the completion of 24 hours of UV irradiation. Thus, the synthesis of nicotine salts appears to be a remarkably general approach for preventing photodriven degradation.

Conclusions

When (S)-nicotine is combined with orotic acid, the resulting salt forms a hemihydrate with the oxygen atoms of the waters residing on C_2 rotation axes. The structure exhibits a complex hydrogen bonding network of discrete and ring-type graph sets form layers that run along [100] and then stack through Van der Waals interactions along [010]. The orotate salt possesses a melting point of 135.5 ℃ which corresponds to a ΔT_m value of 215.4 ℃, the highest ΔT_m value for a nicotine co-crystal or salt reported thus far.

Similar to other nicotine salts, the orotate salt exhibited no degradation after 24 hours of UV irradiation. Thus the crystallization of nicotine appears to be a highly effective means of producing nicotine-based materials with improved resistance to photodegradation whilst also providing the ability to generate materials with tunable thermal properties which is critical for real-world applications. That the crystal engineering may be performed with salt-formers that are food additives or GRAS compounds, and thermally degrade into safe by-products, represents an important step in the production of safer nicotine products.

Experimental

Materials

(S)-nicotine (98%) and orotic acid (97%) were each purchased from Alfa Aesar. Anhydrous absolute ethanol (200 proof, ACS-grade) was purchased from Pharmco by Greenfield Global. Dimethyl sulfoxide-D6 (D, 99.9%) and Methanol-D4 (D, 99.8%) were purchased from Cambridge Isotope Laboratories, Inc. Deionized water was obtained through the use of an in-house 7 stage reverse osmosis system.

Salt Synthesis

(S)-nicotinium orotate hemihydrate was synthesized using a modified slow evaporation set up. Orotic acid (3.1340 g, 20 mmol) was added to a 1 L beaker containing 850 mL of boiling DI water. The mixture was stirred for 1 hour to allow for full dissolution of the salt former. The solution was removed from heat and allowed to cool, after which (S)-nicotine (3.2 mL, 20 mmol) was added in the dark to avoid any potential degradation. The solution was evaporated with air being blown across the solvent to accelerate evaporation. After about 2 days, the resulting slurry, was rinsed with absolute ethanol and collected via vacuum filtration. The crude material was dried via vacuum on a Schlenk line yielding a powdery crystalline product (6.3769 g, 97.41 % yield).

Single Crystal X-ray Diffraction (SC-XRD)

X-ray diffraction data was collected using a Bruker SMART APEX-II CCD diffractometer installed at a rotating anode source (MoKα radiation, λ = 0.71073 Å) and equipped with an Oxford Cryosystems (Cryostream700) nitrogen gas-flow apparatus. Five sets of data (360 frames each) were collected by the rotation method with 0.5° frame-width (ω scans) with 2.0 second exposure times for the single crystalline sample. The sample was run at 90 K. Using Olex2, the structure was solved with intrinsic phasing via the ShelXT structure solution program and refined with the ShelXL software suite using least squares minimization.[34-36] Images of the structures were created using Olex2 and the Mercury 4.0 2021.2.0 visualization and analysis of crystal structures software suite.[37] Absolute configuration was assigned based upon the stereochemistry of the API (S)-nicotine. The flack parameter was removed in accordance with IUCr standards for reporting a structure in which the absolute configuration is assigned based upon a known reference molecule, which in this structure is (S)-nicotine.

Powder X-ray Diffraction (PXRD)

Powder X-ray diffraction data was collected using a Rigaku Ultima IV X-ray Diffraction (XRD) System equipped with standard attachment (CuKα radiation, λ = 1.54 Å). Data collection was done over the 2θ range from 2° to 45° utilizing a 0.02° incremental step. A scanning speed of 5° per minute was utilized. Slit Heights were set as follows: divergence slit: 2/3°; divergence height limiting slit: 10mm; scattering slit: 2/3°; receiving slit: 0.3mm. PXRD patterns were simulated using the Mercury 4.0 2021.2.0 visualization and analysis of crystal structures software suite.[37] A 0.02° was utilized for the simulated PXRD pattern along with a full width half max of 0.1.

Crystal Melting Points

A Stuart SMP10 melting point apparatus was utilized to measure the melting point of the synthesized compounds. 4 replicates were run for the salt.

Differential Scanning Calorimetry

A differential scanning calorimeter, model DSC Q200 (TA Instrument, USA) was used to measure the thermal transitions of the sample. About 10 mg of the synthesized compound was placed into an aluminium pan and sealed. The salt was scanned from 0 °C to above the melting point observed on the Stuart SMP10 at 20 °C/min under argon and nitrogen flow (10 mL/min. each) for 2 full cycles. Enthalpy of fusion was computed from the integrated area under the curve and the entropy of fusion computed by applying Gibbs' free energy in accordance with equilibrium between the solid and liquid state being achieved at the fusion point. A simple DSC scan of the salt former orotic acid was done from 0 ℃ to 410 ℃ to assess the endothermic melting transition temperature utilizing parameters similar to the salt.

UV Photodegradation

NMR analysis was done on a representative sample of the salt former orotic acid, (S)-nicotine, and the synthesized (S)-nicotinium orotate hemihydrate salt. Each sample was then irradiated with ultraviolet (UV) light in a home built vented box with air flow for 24 hours using four Southern New England Ultraviolet Company RPR – 3000A UV bulbs (λ = 300 nm). NMR analysis was then carried out on each sample to screen for any UV photodegradation of products.

Nuclear Magnetic Resonance (NMR)

NMR analysis was run on a Varian Inova-400 broadband spectrometer (400 MHz), using the deuterated solvent appropriately labelled in each spectrum. Spectra were normalized to an intensity of 100. 80 transients were run on each UV stress tested sample.

Hirshfeld Surface Analysis

The Hirshfeld surface of (S)-nicotinium orotate hemihydrate and the previously synthesized nicotinium malate salts was generated using *Crystal Explorer 17.5*.[38] For all salts the d_{norm} surface was mapped using the color scale with the range −0.050 a.u. (red) to 0.600 a.u. (blue). In addition, 2-D fingerprint plots were generated as the outer nuclei (d_e) versus the inner nuclei (d_i) using an expanded interaction distance ranging from 0.6 Å to 2.8 Å.

Author Contributions

Devin J. Angevine: data curation, formal analysis, writing – original draft. Kristine Joy Camacho and Javid Rzayev: data curation. Jason B. Benedict: project administration, funding acquisition, writing – review & editing.

Conflicts of interest

The authors declare no conflicts of interest in the work. The final version of this manuscript has been approved by all authors.

Acknowledgements

Funding for DJA and JBB was provided by: National Science Foundation, Directorate for Mathematical and Physical Sciences (award No. DMR-2003932).

References

1. S. L. Morissette, O. Almarsson, M. L. Peterson, J. F. Remenar, M. J. Read, A. V. Lemmo, S. Ellis, M. J. Cima and C. R. Gardner, *Adv. Drug Delivery Rev.*, 2004, **56**, 275-300.
2. R. J. Dinis-Oliveira, *Biomed Res Int*, 2018, **2018**, 6852857-6852857.
3. A. Bacchi, D. Capucci, M. Giannetto, M. Mattarozzi, P. Pelagatti, N. Rodriguez-Hornedo, K. Rubini and A. Sala, *Crystal Growth & Design*, 2016, **16**, 6547-6555.
4. M. Serafini, S. Cargnin, A. Massarotti, T. Pirali and A. A. Genazzani, *Journal of Medicinal Chemistry*, 2020, **63**, 10170-10187.
5. L. A. Trissel, in *Handbook on Injectable Drugs*, 2007, pp. 1720-1720.
6. D. I. G. University of Illinois at Chicago College of Pharmacy, *Hosp Pharm*, 2014, **49**, 136-163.
7. C. H. Rayburn, W. R. Harlan and H. R. Hanmer, *Journal of the American Chemical Society*, 1941, **63**, 115-116.
8. E. Adamek, M. Goniewicz, W. Baran and A. Sobczak, *CHEM*, 2015, DOI: 10.5171/2015.157781, 1-5.
9. D. H. Volman, G. S. Hammond and K. Gollnick, *Advances In Photochemistry*, John Wiley & Sons, 2009.
10. J. F. Pankow, K. Kim, K. J. McWhirter, W. Luo, J. O. Escobedo, R. M. Strongin, A. K. Duell and D. H. Peyton, *PLoS One*, 2017, **12**, e0173055/0173051-e0173055/0173010.
11. WO2015183801A1, 2015.
12. US20160185750A1, 2016.
13. WO2017089931A1, 2017.
14. US20180051002A1, 2018.
15. WO2019049049A1, 2019.
16. WO2021126313, 2021.
17. D. Capucci, D. Balestri, P. P. Mazzeo, P. Pelagatti, K. Rubini and A. Bacchi, *Cryst. Growth Des.*, 2017, **17**, 4958-4964.
18. A. Scalbert, C. Andres-Lacueva, M. Arita, P. Kroon, C. Manach, M. Urpi-Sarda and D. Wishart, *Journal of Agricultural and Food Chemistry*, 2011, **59**, 4331-4348.
19. D. S. Wishart, C. Knox, A. C. Guo, R. Eisner, N. Young, B. Gautam, D. D. Hau, N. Psychogios, E. Dong, S. Bouatra, R. Mandal, I. Sinelnikov, J. Xia, L. Jia, J. A. Cruz, E. Lim, C. A. Sobsey, S. Shrivastava, P. Huang, P. Liu, L. Fang, J. Peng, R. Fradette, D. Cheng, D. Tzur, M. Clements, A. Lewis, A. De Souza, A. Zuniga, M. Dawe, Y. Xiong, D. Clive, R. Greiner, A. Nazyrova, R. Shaykhutdinov, L. Li, H. J. Vogel and I. Forsythe, *Nucleic Acids Research*, 2008, **37**, D603-D610.
20. J. J. Naveja, M. P. Rico-Hidalgo and J. L. Medina-Franco, *F1000Res*, 2018, **7**, Chem Inf Sci-993.
21. N. Garg, A. Sethupathy, R. Tuwani, R. Nk, S. Dokania, A. Iyer, A. Gupta, S. Agrawal, N. Singh, S. Shukla, K. Kathuria, R. Badhwar, R. Kanji, A. Jain, A. Kaur, R. Nagpal and G. Bagler, *Nucleic Acids Res*, 2018, **46**, D1210-d1216.
22. G. A. Burdock and I. G. Carabin, *Toxicol. Lett.*, 2004, **150**, 3-18.

23. J. B. Hallagan, R. L. Hall and J. Drake, *Food and Chemical Toxicology*, 2020, **138**, 111236.
24. D. J. Angevine, K. J. Camacho, J. Rzayev and J. B. Benedict, *Crystal Growth & Design*, 2022, **22**, 1594-1603.
25. F. Rosenfeldt, *Cardiovascular Drugs and Therapy*, 1998, **12**, 147-152.
26. A. J. Cruz-Cabeza, *CrystEngComm*, 2012, **14**, 6362-6365.
27. C. Alvarez-Lorenzo, A. Castiñeiras, A. Frontera, I. García-Santos, J. M. González-Pérez, J. Niclós-Gutiérrez, I. Rodríguez-González, E. Vílchez-Rodríguez and J. K. Zaręba, *CrystEngComm*, 2020, **22**, 6674-6689.
28. A. Sharfalddin, B. Davaasuren, A.-H. Emwas, M. Jaremko, Ł. Jaremko and M. Hussien, *PLoS One*, 2020, **15**, e0239200.
29. L. H. Al-Wahaibi, J. Joubert, O. Blacque, N. H. Al-Shaalan and A. A. El-Emam, *Scientific Reports*, 2019, **9**, 19745.
30. M. A. Spackman and D. Jayatilaka, *CrystEngComm*, 2009, **11**, 19-32.
31. G. Perlovich, *CrystEngComm*, 2015, **17**.
32. N. Borduas, J. G. Murphy, C. Wang, G. da Silva and J. P. D. Abbatt, *Environmental Science & Technology Letters*, 2016, **3**, 327-331.
33. T. A. Henry, *The Plant Alkaloids*, 4th edn., 1949.
34. G. Sheldrick, *Acta Crystallographica Section A*, 2015, **71**, 3-8.
35. G. Sheldrick, *Acta Crystallographica Section C*, 2015, **71**, 3-8.
36. O. V. Dolomanov, L. J. Bourhis, R. J. Gildea, J. A. K. Howard and H. Puschmann, *Journal of Applied Crystallography*, 2009, **42**, 339-341.
37. C. F. Macrae, I. Sovago, S. J. Cottrell, P. T. A. Galek, P. McCabe, E. Pidcock, M. Platings, G. P. Shields, J. S. Stevens, M. Towler and P. A. Wood, *Journal of Applied Crystallography*, 2020, **53**, 226-235.
38. P. R. Spackman, M. J. Turner, J. J. McKinnon, S. K. Wolff, D. J. Grimwood, D. Jayatilaka and M. A. Spackman, *Journal of Applied Crystallography*, 2021, **54**, 1006-1011.